RSC Advances

PAPER

View Article Online
View Journal | View Issue

Cite this: *RSC Adv.*, 2019, **9**, 42554

A dinuclear cobalt cluster as electrocatalyst for oxygen reduction reaction†

Yun-Wu Li, Wen-Jie Zhang, Chun-Xia Li, Lin Gu, Hong-Mei Du, Hui-Yan Ma,* Su-Na Wang * and Jin-Sheng Zhao*

Dinuclear metal clusters as metalloenzymes execute efficient catalytic activities in biological systems. Enlightened by this, a dinuclear $\{Co_2^{II}\}$ cluster was selected to survey its ORR (Oxygen Reduction Reaction) catalytic activities. The crystalline $\{Co_2^{II}\}$ possesses defined structure and potential catalytic active centers of $\{CoN_4O_2\}$ sites, which was identified by X-ray single crystal diffraction, Raman and XPS. The appropriate supramolecular porosity combining abundant pyridinic-N and triazole-N sites of $\{Co_2^{II}\}$ catalyst synergistically benefit the ORR performance. As a result, this non-noble metal catalyst presents a nice ORR electrocatalytic activity and abides by a nearly 4-electron reduction pathway. Thus, this unpyrolyzed crystalline catalyst clearly provide precise active sites and the whole defined structural information, which can help researcher to design and fabricate efficient ORR catalysts to improve their activities. Considering the visible crystal structure, a single cobalt center-mediated catalytic mechanism was also proposed to elucidate the ORR process.

Received 5th October 2019
Accepted 13th December 2019

DOI: 10.1039/c9ra08068f

rsc.li/rsc-advances

1. Introduction

Oxygen reduction reaction (ORR) is a critical central reaction in many new energy batteries, such as fuel cells and metal–air batteries.[1,2] The best and widely accepted benchmark catalyst for ORR is noble metal Pt,[3] but cost effectiveness blocks its large-scale commercial applications. So lots of Pt-alloy and Pt-free catalysts, such as PtPb/Pt alloy,[4a] Pt/Co alloy,[4b] Pt/Ni alloy,[4c] Pt/Fe alloy,[4d] transition metal derived nanomaterials,[5] carbon species and its composite materials,[6] have been emerging as the times require. Among them, $\{FeN_x\}$ and $\{CoN_x\}$ analogues are two types of high-profile catalysts, due to their competitive ORR catalytic activities and lower cost.[7,8] However, $\{MN_x\}$ (M = Metals) catalysts are usually prepared by pyrolysis of specific precursors, such as coordination multinuclear clusters (CMCs) and metal–organic frameworks (MOFs), which leads to presenting amorphous state and lacking defined structure. As a result, it brings difficulty to manage actual and definite activity sites in ORR progress. Most recently, several groups began to research crystalline metal coordinated complexes as ORR catalysts and have made some progress. For example, a crystal $\{Ni_3^{II}(HITP)\}$ catalyst with $\{NiN_4\}$ sites showed a good ORR activity and stability but just followed a $2e^-$ process.[9] After then, a mononuclear $\{Co^{II}\}$ coordinated complex and graphene composite with $\{CoNO_4\}$ activity sites for ORR,[10] a family of $\{Co_2^{II}\}$ clusters with $\{CoN_5O\}$ activity sites for ORR,[11] a Co^{II} cluster-based MOF with multiple $\{Co^{II}\}$ centers for ORR,[12] have been successively reported and all displayed promising ORR activities. These meaningful works encourage us to start investigating the coordinated crystalline material for ORR.

Our present interest focus on crystalline dinuclear $\{M_2\}$ clusters as ORR catalysts inspired by their efficient catalytic activities in biological systems, such as many dinuclear metalloenzymes including $\{Fe_2^{II}\}$ hydrogenase and $\{Cu_2^{II}\}$ tyrosinase. So we selected a crystalline $\{Co_2^{II}\}$ cluster reported by our group[13] to perform the ORR catalysis in view of following features: (a) the $\{Co_2^{II}\}$ cluster bearing defined crystal structure; (b) the $\{Co_2^{II}\}$ cluster containing precised potential catalytic active center $\{CoN_4O_2\}$ cores; (c) the N-rich ligand in $\{Co_2^{II}\}$ cluster simultaneous involving pyridinic-N and triazole-N sites; (d) the $\{Co_2^{II}\}$ cluster possessing thermal stability.[13] Theses characteristics could theoretically endow the $\{Co_2^{II}\}$ cluster with targeted ORR activity, and as expected, it can boost the ORR and abides by a nearly 4-electrons reduction pathway. This unpyrolyzed non-noble metal crystalline catalyst here clearly provide precise active sites and the whole defined structural information, which can help researcher to design and fabricate efficient ORR catalysts to improve their activities.

Shandong Provincial Key Laboratory/Collaborative Innovation Center of Chemical Energy Storage and Novel Cell Technology, School of Chemistry and Chemical Engineering, Liaocheng University, Liaocheng 252000, P. R. China. E-mail: mahuiyanyan@163.com; wangsuna@lcu.edu.cn; j.s.zhao@163.com

† Electronic supplementary information (ESI) available. See DOI: 10.1039/c9ra08068f

2. Experimental section

2.1 Chemicals and syntheses

All chemicals were purchased without purification. Dinuclear $\{Co_2^{II}\}$ (molecular formula: $[Co(pmmat)ClO_4]_2$) cluster catalyst

was synthesized according our reported experiment and the detailed see ESI.† [13]

2.2 Material characterization

N_2 adsorption experiment was tested using a Micrometrics ASAP 2020M. Electron microscopy measurements were measured using field-emission scanning electron microscopy (SEM, JSM-6360). Transmission electron microscopy (TEM) was measured by JEM-2100 at 200 kV. Raman spectrum was tested using Monovista CRS500. X-ray photoelectron spectrum (XPS) were carried out using ESCALAB Xi+. Elemental analyses (C, H and N) were performed on an Elementar Vario EL analyzer. The X-ray powder diffraction (XRPD) was obtained on a D/MAX-rA (Rigaku) diffractometer with Cu Kα radiation (λ = 1.542 Å) with a scan rate of 4° min^{-1}. FT-IR spectra were recorded on a FT6700 spectrometer (USA) using KBr disc method in the range of 400–4000 cm^{-1}.

2.3 Electrochemical measurements

The electrocatalytic properties including EIS (electrochemical impedance spectroscopy) were conducted using an Autolab PGSTAT 302 N potentiostat, equipped with an electrode rotator (AFMSRCE, Pine). A typical experiment: 1.6 mg $\{Co_2^{II}\}$ catalyst and 1.6 mg high-purity carbon powder (only 3.2 mg 20% Pt/C) were dispersed in a mixture of 570 μL ultra-pure H_2O and 177 μL iso-propanol under supersound, and 3 μL 5 wt% Nafion dispersed ethanol solution was added. Then, 8.5 μL catalyst ink was dropped on the glassy carbon rotating disk electrode (RDE) and air dried. So the mass loading of the $\{Co_2^{II}\}$ and Pt/C catalysts on the electrodes are 18.13 μg and 36.26 μg, respectively. The corresponding metal Co and Pt loading is 2.14 μg and 7.25 μg, respectively. A three-electrode cell system was worked in 70 mL 0.1 M KOH electrolyte. The working electrode is RDE glassy carbon, the reference electrode is saturated Ag/AgCl, and the counter electrode is platinum wire. Cyclic voltammogram (CV) and linear sweep voltammogram (LSV) tests were performed with a scan rate of 100 and 5 mV s^{-1}, respectively. For comparison, commercial Pt/C was also loaded onto the RDE by the same method. All the potentials were referred to a reversible hydrogen electrode (RHE) using equation $E_{RHE} = E_{Ag/AgCl}$ + 0.197 V + 0.0591 pH.

The ORR kinetics was analyzed with the Koutecky–Levich (K–L) plots based on K–L equations:

$$\frac{1}{J} = \frac{1}{J_K} + \frac{1}{J_L} = \frac{1}{J_K} + \frac{1}{B\omega^{1/2}} \quad (1a)$$

$$B = 0.62nFC^*_{O_2} D_{O_2}{}^{2/3} \nu^{-1/6} \quad (1b)$$

$$J_K = nFkC^*_{O_2} \quad (1c)$$

where J, J_K, and J_L is the measured, kinetic and diffusion limiting current densities (mA cm^{-2}), respectively. ω is the electrode rotating speed (rad s^{-1}). B is the reciprocal of the slope determined from the K–L plots, and n is the number of electrons transferred per oxygen molecule. F is the Faraday constant (96 485 C mol^{-1}); D is the diffusion coefficient of O_2 in 0.1 M KOH (1.9×10^{-5} cm^2 s^{-1}); ν is the kinetic viscosity (0.01 cm^2 s^{-1}), k is the electron transfer rate constant, and C^* is the concentration of O_2 (1.2×10^{-6} mol cm^{-3}) in solution.

3. Results and discussions

3.1 The structure and component of the $\{Co_2^{II}\}$ catalyst

The precise structure of catalyst is a dinuclear $\{Co_2^{II}\}$ cluster with two $\{CoN_4O_2\}$ coordinated cores wrapped by two N-rich organic ligands pmmat$^-$ (Fig. 1a).[13] The detailed crystal data are shown in Table S1 (ESI†). It displays a 3D supramolecular microporous structure with a 21.3% porosity using the PLATON analysis (Fig. 1b), which can favor O_2 transport during ORR process. The porous fact also proved by the N_2 adsorption at 77 K and 1 atm (Fig. 2a). The adsorb amount of N_2 increases slowly before 0.5 atm, and then rises rapidly to achieve a maximum at 63.3 cm^3 g^{-1}. The relevant BET (Brunner–Emmett–Teller) surface areas is 134.2 m^2 g^{-1} by calculated using above N_2 adsorption data. The pore size diameter is among 1.5–15 Å, and the medium diameter is 3.9 Å, which can accommodate N_2 (kinetic diameter: 3.6 Å) and O_2 (kinetic diameter: 3.5 Å) appropriately.[14] The other basic characterization containing IR, PXRD, magnetism, and TG, can confirm its single crystalline pure-phase and thermal stability.[13] The SEM and TEM images show the $\{Co_2^{II}\}$ catalyst displays a flake-like morphology with crystalline smooth surface (Fig. 1c and d). The width is *ca.* 3–5 μm and length is *ca.* 30–50 μm.

The Raman spectrum further confirms the catalyst is in crystalline state and composed of various functional modules (Fig. 2b).[15] It displays five main peaks locating at 268, 690, 1365, 1603, and 2656 cm^{-1}, respectively. The low-frequency peak at 268 cm^{-1} is mainly attributed to the lattice vibrations of the $\{Co_2^{II}\}$ catalyst.[15] In the fingerprint region, the peaks at 690 and 1365 cm^{-1} are mainly due to the $\{Co_2^{II}\}$ cluster breathing, pyridine and triazole rings contracting, and C–H stretching; the peak at 1603 cm^{-1} may result from pyridine and triazole rings

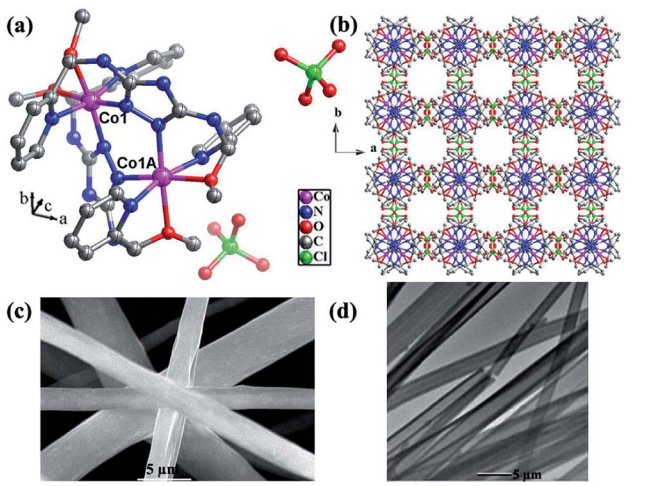

Fig. 1 (a) The structure of $\{Co_2^{II}\}$ catalyst. (b) The 3D supramolecular packing mode along *c* axis showing supramolecular porosity. (c) The SEM and (d) TEM images of $\{Co_2^{II}\}$ catalyst.

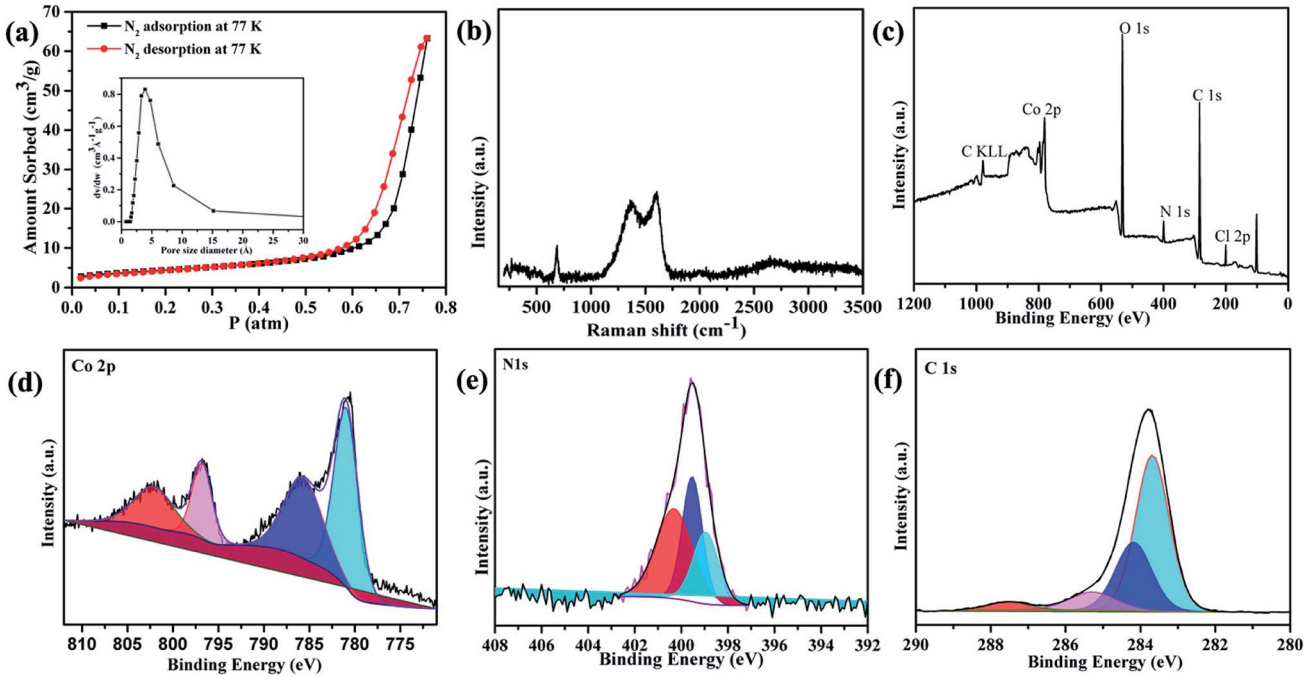

Fig. 2 (a) N_2 adsorption at 77 K and 1 atm (inset: the pore size diameter). (b) Raman spectrum. (c–f) XPS spectrum of $\{Co_2^{II}\}$ catalyst.

breathing and C–H bending.[15] The high-frequency peak at 2656 cm^{-1} can be attributed to the C–O stretching of the organic groups. The C–N–C stretching is overlapped by strong intensities at 1365 and 1603 cm^{-1}.

To further prove the chemical composition and oxidation states of the catalyst, the XPS were measured (Fig. 2c–f). The overall spectrum shows there exist Co, C, N, O and Cl elements (Fig. 2c). The high resolution of Co2p spectrum reveals it contains four typical characteristic peaks which are assigned to Co(II)$2p_{3/2}$ (780.2 eV), Co(II)$2p_{1/2}$ (796 eV), and two satellite peaks (786 and 802 eV) (Fig. 2d), respectively.[16,17] The high resolution of N1s spectra are divided into three peaks (Fig. 2e). The peak at 398.96 eV is the pyridinic N species (24.08%), 399.53 eV is the amino group N species (33.15%), and 400.31 eV is the triazole N species (42.77%), respectively.[16,17] As references reported, the pyridinic-N and triazole-N can synergistically offer ORR active sites.[16,17] The high resolution of C1s spectrum can be deconvoluted into four peaks at 283.68, 284.18, 287.52, and 285.29 eV (Fig. 2f), regarding as C–C, C=C, C=N/C–O, and C–N/C=O, respectively.[16,17] The XPS results are aligned with the X-ray single crystal structure analysis.[13]

3.2 ORR electrocatalytic activities

The stability of the catalyst in the ink is important. We soaked the crystals of as-synthesised catalyst in a similar mixture solution including the same ratio of H_2O/iso-propanol/ethanol under supersound. After 2 days, we filtered the catalyst and carried out the PXRD test. The PXRD patterns indicate that the soaked catalyst also has crystalline forms (Fig. S3, ESI†), which can proved the stability and insolubility of the catalyst in the ink.

Then, the ORR activities of the crystal $\{Co_2^{II}\}$ cluster and 20% Pt/C were both tested under the same condition. The CV curves exhibit an obvious oxygen redox peak in O_2-saturated electrolyte compared with N_2 environment (Fig. 3a), which reveals the potential ORR activities of the $\{Co_2^{II}\}$ catalyst. From LSV curves of the $\{Co_2^{II}\}$ catalyst (Fig. 3b), the limiting current densities (J_L) increase evidently along with the raising rotation rates from 400 to 1600 rpm. J_L reaches maximum value of 4.43 mA cm^{-2} at highest rotation rate 1600 rpm, implying the fastest O_2 diffuse around the electrode surface. As seen, the onset potential (E_{onset}) and half-wave potential ($E_{1/2}$) is 1.05 and 0.79 mV for the $\{Co_2^{II}\}$ catalyst, respectively. For comparison, the LSV curves of commercial Pt/C in same condition show similar trend (Fig. 3c). From the curves, the activities of $\{Co_2^{II}\}$ catalyst are a little weaker than Pt/C catalyst, whereas the maximum J_L, E_{onset}, and $E_{1/2}$ of Pt/C is 4.76 mA cm^{-2}, 1.15 mV, and 0.93 mV for Pt/C, respectively. From references, crystalline coordinated clusters possessing high ORR activities are rare.[9–11] Furthermore, Koutecky–Levich (K–L) equation was used to evaluate kinetic progress of the $\{Co_2^{II}\}$ catalyst (Fig. 3d).[18] From fitted data at various potentials from 0 to 0.20 V, the K–L curves present fine linearity with almost the same slopes. By calculated, the consistent electron transfer number (n) is 3.8, theoretically corresponding to a four-electrons reduction pathway. The good linearity also illustrates the ORR of the $\{Co_2^{II}\}$ catalyst following the first-order reaction kinetics. The kinetic current density (J_K) of the $\{Co_2^{II}\}$ catalyst is *ca.* 20.72 mA cm^{-2} according to K–L curves at 0.20 V. The n and J_K is near Pt/C (where $n = 4.0$, $J_K = 22.33$ mA cm^{-2}, Fig. 3e and f) at the same condition, which further confirms the good ORR activities of the $\{Co_2^{II}\}$ catalyst. The various electrochemical parameters of the $\{Co_2^{II}\}$ catalyst for

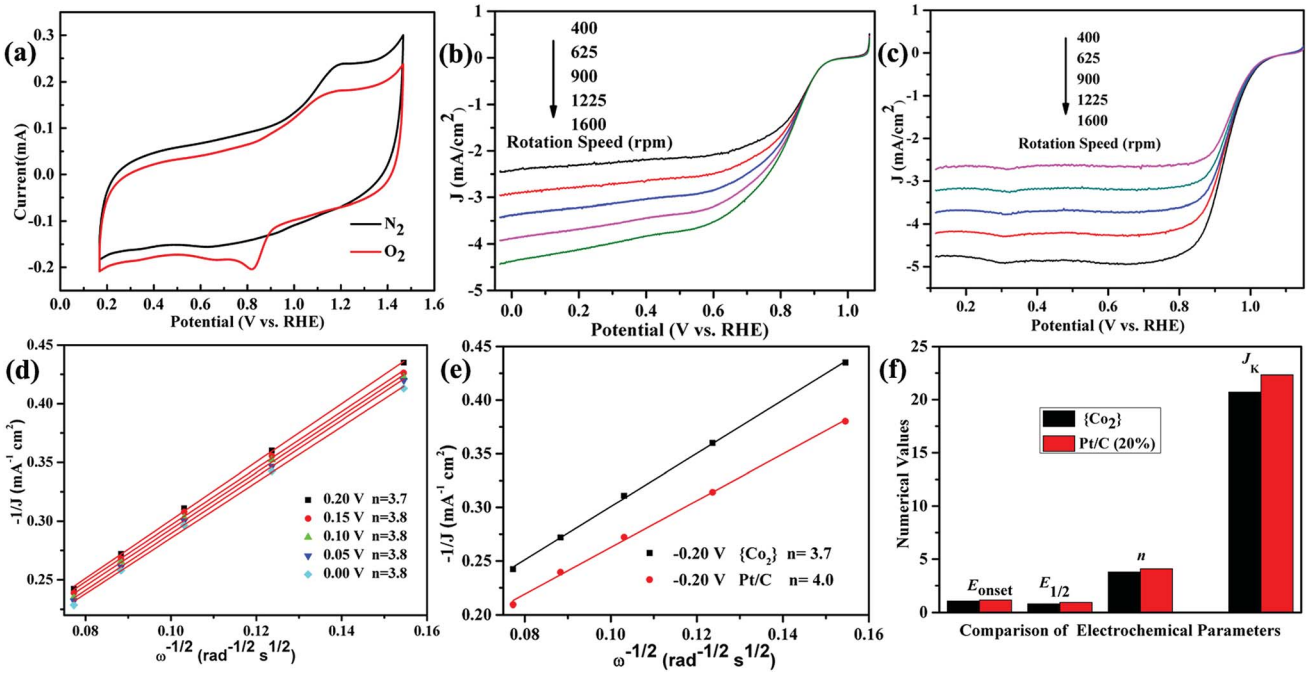

Fig. 3 (a) CV curves of the $\{Co_2^{II}\}$ catalyst. (b) and (c) LSV curves of the $\{Co_2^{II}\}$ catalyst and commercial Pt/C. (d) K–L plots of the $\{Co_2^{II}\}$ catalyst at different potentials from 0 to 0.20 V. (e) Comparison K–L plots of the $\{Co_2^{II}\}$ catalyst and commercial Pt/C at 0.2 V. (f) The comparison various electrochemical parameters including E_{onset}, $E_{1/2}$, n and J_K of the $\{Co_2^{II}\}$ catalyst and commercial Pt/C.

evaluating the ORR performance containing E_{onset}, $E_{1/2}$, n, and J_K, are listed in column in order to help comparing with Pt/C (Fig. 3f).

The long-term durability of $\{Co_2^{II}\}$ catalyst and the 20% commercial Pt/C was also evaluated by chronoamperometric measurements in O_2 saturated 0.1 M KOH solutions. As revealed in the current–time (i–t) curves (Fig. 4a), $\{Co_2^{II}\}$ catalyst retains 83% of the initial current after 36 000 seconds, whereas the value for the commercial Pt/C is only 73%, indicating that $\{Co_2^{II}\}$ catalyst exhibits better stability than the Pt/C in alkaline solution. Moreover, the EIS was further performed to investigate the catalytic kinetics of $\{Co_2^{II}\}$ catalyst and commercial Pt/C. As shown in Fig. 4b, the Nyquist plots and the simulated equivalent circuits were presented for the two catalysts. As known, the radius of Nyquist plot can reflect the charge transfer resistance (R_p) and further to evaluate the ORR electrocatalytic activity. The R_p of $\{Co_2^{II}\}$ catalyst (432 Ω) is higher than commercial Pt/C (228 Ω), which is consistent with the slightly worse ORR performance of $\{Co_2^{II}\}$ catalyst compared to commercial Pt/C. Hence, the $\{Co_2^{II}\}$ catalyst is one efficient ORR catalyst with good stability and electrocatalytic activity.

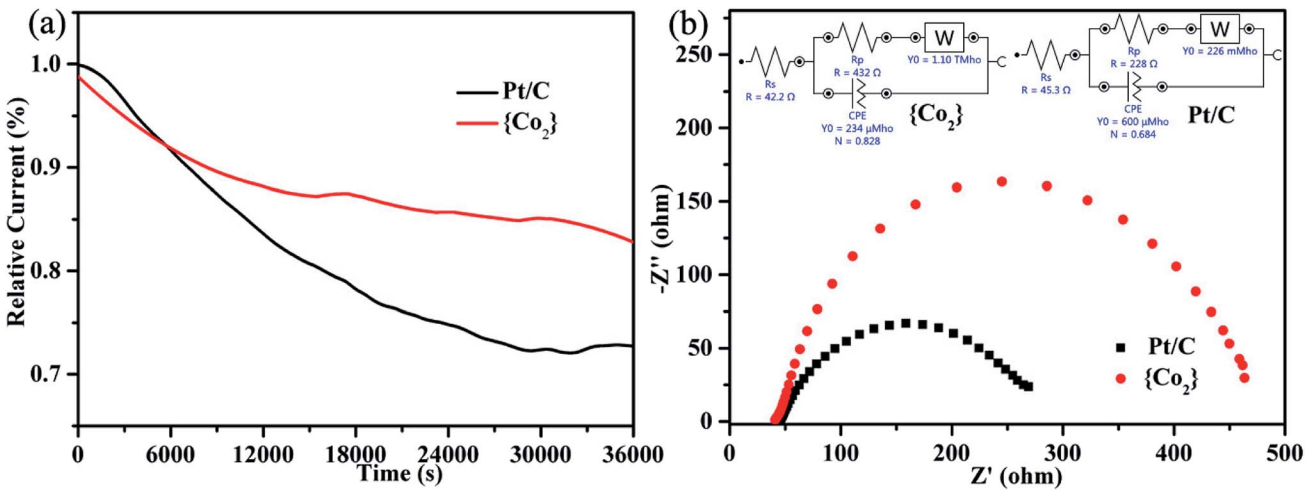

Fig. 4 (a) The current–time (i–t) chronoamperometry curves of $\{Co_2^{II}\}$ catalyst and commercial Pt/C in O_2-saturated 0.1 M KOH solution.(b) Nyquist plots of EIS for $\{Co_2^{II}\}$ catalyst and commercial Pt/C (inset: simulated equivalent circuits).

For comparison, we also tested the ORR activities of the free ligand Hpmat in the same condition. As shown from the Fig. S4 (ESI†), the corresponding parameters E_{onset}, $E_{1/2}$, n, and J_K are worse than the $\{Co_2^{II}\}$ catalyst. So it can be speculated that the Co^{II}-coordinated centres of the $\{Co_2^{II}\}$ cluster will be the catalytic active sites. Combination of X-ray single crystal structure analysis, XPS results, the worse ORR activities of the free ligand, and the references including experimental and theoretical insights,[7,8,19,20] it can be speculation that the ORR active sites of the $\{Co_2^{II}\}$ catalyst are probable the $\{CoN_4O_2\}$ coordinated cores.[7,8,10,12,19,20]

Stated thus, the good ORR activities of $\{Co_2^{II}\}$ catalyst may be attributed to the following two factors: on one hand, the appropriate porosity and the BET surface area provide effective mass transport pathway for the defined Co^{II}-coordinated $\{CoN_4O_2\}$ active sites.[7,8,10,12,16,17,19,20] On the other hand, the abundant pyridinic-N and triazole-N synergistically benefit the ORR activities.[7,8,16,17,19,20] These two types of N not only can enhance the efficient electron transfer, but also lead to more defects and positive $\{CoN_4O_2\}$ active sites, which can both improve the ORR performance.[7,8,10,12,16,17,19,20] To date, most ORR researches are focus on pyrolysis various precursors (such as CMCs and MOFs) to obtain $\{MN_x\}$ catalysts, their precise active sites and the catalytic mechanism are still not very clear, although they show higher ORR performance. In comparison, unpyrolyzed coordinated polymers (including CMCs and MOFs) often display slightly worse ORR activities, but they can provide precise active sites and the whole structural information, which can help researcher to design and fabricate efficient ORR catalysts to improve their activities.

3.3 The proposed ORR electrocatalytic mechanism

Considering the nearly symmetric structure and coordination environment of the two Co^{II} ions, a single cobalt center-mediated reduction mechanism was proposed, which abides by a four-electron reduction pathway (see Fig. 5).[10–12,21–25]

(1): $[Co^{II}Co^{II}L_2]^{2+}$ (abbr. **1**) catalyst captures one OH^- in a alkaline solution to form a $[Co^{II}Co^{II}(OH)L_2]^+$ intermediate abbreviated as **1a**, the reaction equation is:

$$[Co^{II}Co^{II}L_2]^{2+} + OH^- \rightarrow [Co^{II}Co^{II}(OH)L_2]^+ \quad (2a)$$

(2): **1a** containing $[Co^{II}Co^{II}(OH)L_2]^+$ adsorbs one O_2 molecule on active sites and releases one OH^-, generating a $[Co^{II}Co^{II}(O{=}O)L_2]^{2+}$ intermediate abbreviated as **1b**, the reaction equation is:

$$[Co^{II}Co^{II}(OH)L_2]^+ + O_2 \rightarrow [Co^{II}Co^{II}(O{=}O)L_2]^{2+} + OH^- \quad (2b)$$

(3): O_2 is feasible to oxidize one Co^{II} ion to Co^{III} ion, and transfers to a $[Co^{II}Co^{III}(O–O)L_2]^{2+}$ intermediate abbreviated as **1c**, the reaction equation is:

$$[Co^{II}Co^{II}(O{=}O)L_2]^{2+} \rightarrow [Co^{II}Co^{III}(O–O)L_2]^{2+} \quad (2c)$$

(4): $[Co^{II}Co^{III}(O–O)L_2]^{2+}$ fixes one H_2O molecule and obtains one electron at the same time releases one OH^-, generating a $[Co^{II}Co^{III}(O–OH)L_2]^{2+}$ intermediate abbreviated as **1d**, the reaction equation is:

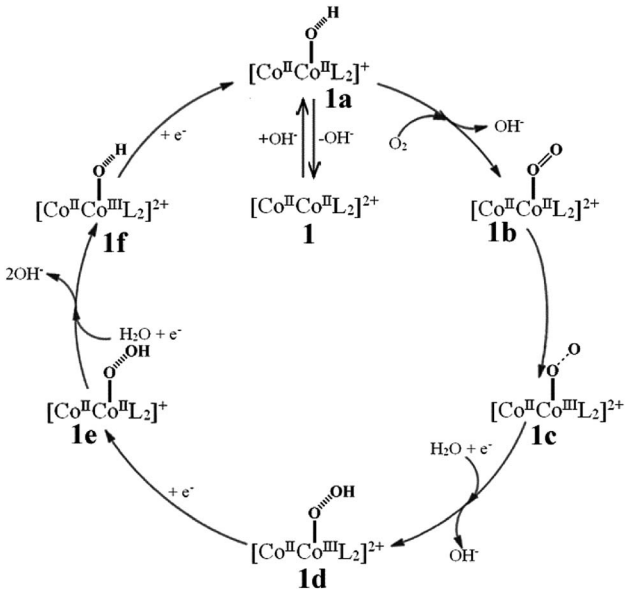

Fig. 5 The proposed ORR mechanism of the $\{Co_2^{II}\}$ catalyst in alkaline medium.

$$[Co^{II}Co^{III}(O–O)L_2]^{2+} + H_2O + e^- \rightarrow [Co^{II}Co^{III}(O–OH)L_2]^{2+} + OH^- \quad (2d)$$

(5): $[Co^{II}Co^{III}(O–OH)L_2]^{2+}$ continuously obtains one electron to reduce the Co^{III} to Co^{II} and generates a $[Co^{II}Co^{II}(O–OH)L_2]^+$ intermediate abbreviated as **1e**, the reaction equation is:

$$[Co^{II}Co^{III}(O–OH)L_2]^{2+} + e^- \rightarrow [Co^{II}Co^{II}(O–OH)L_2]^+ \quad (2e)$$

(6): $[Co^{II}Co^{II}(O–OH)L_2]^+$ further fixes one H_2O molecule and obtains one electron at the same time releases two OH^-, generating a $[Co^{II}Co^{III}(OH)L_2]^{2+}$ intermediate abbreviated as **1f**, the reaction equation is:

$$[Co^{II}Co^{II}(O–OH)L_2]^+ + H_2O + e^- \rightarrow [Co^{II}Co^{III}(OH)L_2]^{2+} + 2OH^- \quad (2f)$$

(7): $[Co^{II}Co^{III}(OH)L_2]^{2+}$ further obtains one electron to reduce Co^{III} ion into Co^{II} ion, returning to $[Co^{II}Co^{II}(OH)L_2]^+$ **1a** intermediate, the reaction equation is:

$$[Co^{II}Co^{III}(OH)L_2]^{2+} + e^- \rightarrow [Co^{II}Co^{II}(OH)L_2]^+ \quad (2g)$$

(8): the $[Co^{II}Co^{II}(OH)L_2]^+$ releases the OH^- and goes back to $[Co^{II}Co^{II}L_2]^{2+}$ **1**, completing one catalytic cycle progress:

$$[Co^{II}Co^{II}(OH)L_2]^+ \rightarrow [Co^{II}Co^{II}L_2]^{2+} + OH^- \quad (2h)$$

4. Conclusion

In conclusion, a Pt-free dinuclear $\{Co_2^{II}\}$ cluster was elaborately selected to research its ORR catalytic activities inspired by dinuclear metalloenzymtic catalysis in biological systems. The

$\{Co_2^{II}\}$ catalyst possesses defined crystal structure, precised $\{CoN_4O_2\}$ potential catalytic active centers, N-rich ligand involving pyridinic-N and triazole-N, and thermal stability. These features endow the $\{Co_2^{II}\}$ catalyst with a nice ORR electrocatalytic performance by a nearly 4-electrons reduction pathway. Considering the visible crystal structure, a single cobalt center-mediated catalytic mechanism was also proposed to elucidate the ORR process, which can help researcher to design and fabricate efficient ORR catalysts to improve their activities.

Conflicts of interest

There are no conflicts to declare.

Acknowledgements

This work was financially supported by the NNSF of China (21771095, 21571092 and 21601079), the NSF of Shandong Province (ZR2017JL013), and the Youth Innovation Team of Shandong Colleges and Universities (2019KJC027).

References

1 (*a*) R. Devanathan, *Energy Environ. Sci.*, 2008, **1**, 101–119; (*b*) X. X. Wang, D. A. Cullen, Y. T. Pan, S. Hwang, M. Y. Wang, Z. X. Feng, J. Y. Wang, M. H. Engelhard, H. G. Zhang, Y. H. He, Y. Y. Shao, D. Su, K. L. More, J. S. Spendelow and G. Wu, *Adv. Mater.*, 2018, **30**, 1706758.

2 (*a*) T. M. Gür, *Energy Environ. Sci.*, 2018, **11**, 2696–2767; (*b*) P. Tan, B. Chen, H. R. Xu, H. C. Zhang, W. Z. Cai, M. Ni, M. L. Liu and Z. P. Shao, *Energy Environ. Sci.*, 2017, **10**, 2056–2080; (*c*) M. H. Yu, Z. K. Wang, C. Hou, Z. L. Wang, C. L. Liang, C. Y. Zhao, Y. X. Tong, X. H. Lu and S. H. Yang, *Adv. Mater.*, 2017, **29**, 1602868.

3 (*a*) J. B. Wu and H. Yang, *Acc. Chem. Res.*, 2013, **46**, 1848–1857; (*b*) L. Zhang, L. T. Roling, X. Wang, M. Vara, M. F. Chi, J. Y. Liu, S. II Choi, J. Park, J. A. Herron, Z. X. Xie, M. Mavrikakis and Y. N. Xia, *Science*, 2015, **349**, 412–416.

4 (*a*) L. Z. Bu, N. Zhang, S. J. Guo, X. Zhang, J. Li, J. L. Yao, T. Wu, G. Lu, J. Y. Ma, D. Su and X. Q. Huang, *Science*, 2016, **354**, 1410–1414; (*b*) W. H. Lai, B. W. Zhang, Z. P. Hu, X. M. Qu, Y. X. Jiang, Y. X. Wang, J. Z. Wang, H. K. Liu and S. L. Chou, *Adv. Funct. Mater.*, 2019, **29**, 1807340; (*c*) C. Chen, Y. J. Kang, Z. Y. Huo, Z. W. Zhu, W. Y. Huang, H. L. L. Xin, J. D. nyder, D. G. Li, J. A. Herron, M. Mavrikakis, M. F. Chi, K. L. More, Y. D. Li, N. M. Markovic, G. A. Somorjai, P. D. Yang and V. R. Stamenkovic, *Science*, 2014, **343**, 1339–1343; (*d*) C. Wang, Y. Hou, J. Kim and S. Sun, *Angew. Chem., Int. Ed.*, 2007, **46**, 6333–6335.

5 (*a*) W. T. Hong, M. Risch, K. A. Stoerzinger, A. Grimaud, J. Suntivich and Y. Shao-Horn, *Energy Environ. Sci.*, 2015, **8**, 1404–1427; (*b*) D. F. Yan, Y. X. Li, J. Huo, R. Chen, L. M. Dai and S. Y. Wang, *Adv. Mater.*, 2017, **29**, 1606459; (*c*) H. J. Qiu, P. Du, K. L. Hu, J. J. Gao, H. L. Li, P. Liu, T. Ina, K. Ohara, Y. Ito and M. W. Chen, *Adv. Mater.*, 2019, **31**, 1900843; (*d*) W. Xia, A. Mahmood, Z. B. Liang, R. Q. Zou and S. J. Guo, *Angew. Chem., Int. Ed.*, 2016, **55**, 2650–2676.

6 (*a*) C. G. Hu and L. M. Dai, *Angew. Chem., Int. Ed.*, 2016, **55**, 11736–11758; (*b*) N. Y. Cheng, L. Ren, X. Xu, Y. Du and S. X. Dou, *Adv. Energy Mater.*, 2018, **8**, 1801257; (*c*) Y. Y. Huang, Y. Q. Wang, C. Tang, J. Wang, Q. Zhang, Y. B. Wang and J. T. Zhang, *Adv. Mater.*, 2019, **31**, 1803800; (*d*) H. T. Sun, L. Mei, J. F. Liang, Z. P. Zhao, C. Lee, H. L. Fei, M. N. Ding, J. Lau, M. F. Li, C. Wang, X. Xu, G. L. Hao, B. Papandrea, I. Shakir, B. Dunn, Y. Huang and X. F. Duan, *Science*, 2017, **356**, 599–604.

7 (*a*) Q. T. Liu, X. F. Liu, L. R. Zheng and J. L. Shui, *Angew. Chem., Int. Ed.*, 2018, **57**, 1204–1208; (*b*) J. Y. Liu, Y. Liu, P. Li, L. H. Wang, H. R. Zhang, H. Liu, J. L. Liu, Y. X. Wang, W. Tian, X. B. Wang, Z. T. Li and M. B. Wu, *Carbon*, 2018, **126**, 1–8; (*c*) P. Peng, L. Shi, F. Huo, C. X. Mi, X. H. Wu, S. J. Zhang and Z. H. Xiang, *Sci. Adv.*, 2019, **5**, eaaw2322; (*d*) F. L. Li, P. T. Wang, X. Q. Huang, D. J. Young, H. F. Wang, P. Braunstein and J. P. Lang, *Angew. Chem., Int. Ed.*, 2019, **58**, 7051–7056.

8 (*a*) M. D. Zhang, Q. B. Dai, H. G. Zheng, M. D. Chen and L. M. Dai, *Adv. Mater.*, 2018, **30**, 1705431; (*b*) J. Zhou, Y. B. Dou, A. W. Zhou, R. M. Guo, M. J. Zhao and J. R. Li, *Adv. Energy Mater.*, 2017, **7**, 1602643; (*c*) Y. P. Wu, J. W. Tian, S. Liu, B. Li, J. Zhao, L. F. Ma, D. S. Li, Y. Q. Lan and X. H. Bu, *Angew. Chem., Int. Ed.*, 2019, **58**, 12185–12189; (*d*) C. H. Liu, Y. J. Tang, X. L. Wang, W. Huang, S. L. Li, L. Z. Dong and Y. Q. Lan, *J. Mater. Chem. A*, 2016, **4**, 18100–18106.

9 E. M. Miner, T. Fukushima, D. Sheberla, L. Sun, Y. Surendranath and M. Dincă, *Nat. Commun.*, 2016, **7**, 10942.

10 J. Han, Y. J. Sa, Y. Shim, M. Choi, N. Park, S. H. Joo and S. Park, *Angew. Chem., Int. Ed.*, 2015, **54**, 12622–12626.

11 C. D. Giovanni, C. Gimbert-Suriñach, M. Nippe, J. Benet-Buchholz, J. R. Long, X. Sala and A. Llobet, *Chem.–Eur. J.*, 2016, **22**, 361–369.

12 P. Mani, A. Sheelam, S. Das, G. X. Wang, V. K. Ramani, K. Ramanujam, S. K. Pati and S. Mandal, *ACS Omega*, 2018, **3**, 3830–3834.

13 H. Y. Ma, Y. W. Li, S. Y. Zeng, S. N. Wang, N. Yang and X. Shao, *J. Cluster Sci.*, 2016, **27**, 1945–1952.

14 (*a*) Y. W. Li, J. Xu, D. C. Li, J. M. Dou, H. Yan, T. L. Hu and X. H. Bu, *Chem. Commun.*, 2015, **51**, 14211–14214; (*b*) Y. W. Li, H. Yan, T. L. Hu, H. Y. Ma, D. C. Li, S. N. Wang, Q. X. Yao, J. M. Dou, J. Xu and X. H. Bu, *Chem. Commun.*, 2017, **53**, 2394–2397; (*c*) D. S. Zhang, Y. Z. Zhang, X. L. Zhang, F. Wang, J. Zhang, H. Hu, J. Gao, H. Yan, H. L. Liu, H. Y. Ma, L. L. Geng and Y. W. Li, *ACS Appl. Mater. Interfaces*, 2019, **11**, 20104–20109; (*d*) H. Y. Ma, Y. Z. Zhang, H. Yan, W. J. Zhang, Y. W. Li, S. N. Wang, D. C. Li, J. M. Dou and J. R. Li, *Dalton Trans.*, 2019, **48**, 13541–13545.

15 (*a*) Y. X. Shen, B. Shan, H. Cai, Y. Qin, A. Agarwal, D. B. Trivedi, B. Chen, L. Liu, H. L. Zhuang, B. Mu and

S. Tongay, *Adv. Mater.*, 2018, **30**, 1802497; (*b*) C. Shi, M. W. Chen, X. Han, Y. F. Bi, L. L. Huang, K. Zhou and Z. P. Zheng, *Inorg. Chem. Front.*, 2018, **5**, 1329–1335.

16 (*a*) R. Z. Zhang, S. J. He, Y. Z. Lu and W. Chen, *J. Mater. Chem. A*, 2015, **3**, 3559–3567; (*b*) Y. Gartia, C. M. Parnell, F. Watanabe, P. Szwedo, A. S. Biris, N. Peddi, Z. A. Nima and A. Ghosh, *ACS Sustainable Chem. Eng.*, 2015, **3**, 97–102; (*c*) X. Qing, J. J Shi, C. Y. Ma, M. Y. Fan, Z. Y. Bai, Z. W. Chen, J. L. Qiao and J. J. Zhang, *J. Power Sources*, 2014, **266**, 88–98.

17 (*a*) J. Y. Liu, L. Xu, Y. L. Deng, Y. L. Deng, X. W. Zhu, J. J. Deng, J. B. Lian, J. J. Wu, J. C. Qian, H. Xu, S. Q. Yuan, H. M. Li and P. M. Ajayan, *J. Mater. Chem. A*, 2019, **7**, 14291–14301; (*b*) D. R. Kumar, S. Kesavan, M. L. Baynosa and J. J. Shim, *Electrochim. Acta*, 2017, **246**, 1131–1140; (*c*) H. Koshikawa, S. Nakanishi, K. Hashimoto and K. Kamiya, *Electrochim. Acta*, 2015, **180**, 173–177.

18 (*a*) P. Strasser, *Acc. Chem. Res.*, 2016, **49**, 2658–2668; (*b*) R. Liu, D. Wu, X. Feng and K. Müllen, *Angew. Chem., Int. Ed.*, 2010, **49**, 2565–2569.

19 (*a*) J. Gao, N. Ma, Y. M. Zheng, J. F. Zhang, J. Z. Gui, C. K. Guo, H. Q. An, X. Y. Tan, Z. Yin and D. Ma, *ChemCatChem*, 2017, **9**, 1601–1609; (*b*) H. Yang, X. Chen, W. T. Chen, Q. Wang, N. C. Cuello, A. Nafady, A. M. Al-Enizi, G. I. N. Waterhouse, G. A. Goenaga, T. A. Zawodzinski, P. E. Kruger, J. E. Clements, J. Zhang, H. Tian, S. G. Telfer and S. Q. Ma, *ACS Nano*, 2019, **13**, 8087–8098.

20 (*a*) Y. Tong, P. Z. Chen, T. P. Zhou, K. Xu, W. S. Chu, C. Z. Wu and Y. Xie, *Angew. Chem., Int. Ed.*, 2017, **56**, 7121–7125; (*b*) X. X. Sun, K. Li, C. Yin, Y. Wang, M. G. Jiao, F. He, X. W. Ba, H. Tang and Z. J. Wu, *Carbon*, 2016, **108**, 541–550.

21 (*a*) C. C. Ren, H. B. Li, R. Li, S. L. Xu, D. H. Wei, W. J. Kang, L. Wang, L. P. Jia, B. C. Yang and J. F. Liu, *RSC Adv.*, 2016, **6**, 33302–33307; (*b*) X. Mao, C. Y. Ling, C. Tang, C. Yan, Z. H. Zhu and A. J. Du, *J. Catal.*, 2018, **367**, 206–211; (*c*) H. C. Li, Y. J. Zhang, X. Hu, W. J. Liu, J. J. Chen and H. Q. Yu, *Adv. Energy Mater.*, 2018, **8**, 1702734; (*d*) Q. Jia, N. Ramaswamy, H. Hafiz, U. Tylus, K. Strickland, G. Wu, B. Barbiellini, A. Bansil, E. F. Holby, P. Zelenay and S. Mukerjee, *ACS Nano*, 2015, **9**, 12496–12505.

22 (*a*) T. Ouyang, H. H. Huang, J. W. Wang, D. C. Zhong and T. B. Lu, *Angew. Chem., Int. Ed.*, 2017, **56**, 738–743; (*b*) T. Ouyang, H. J. Wang, H. H. Huang, J. W. Wang, S. Guo, W. J. Liu, D. C. Zhong and T. B. Lu, *Angew. Chem., Int. Ed.*, 2018, **57**, 16480–16485.

23 (*a*) S. Li, L. Zhang, J. Kima, M. Pan, Z. Shi and J. J. Zhang, *Electrochim. Acta*, 2010, **55**, 7346–7353; (*b*) M. Lions, J. B. Tommasino, R. Chattot, B. Abeykoon, N. Guillou, T. Devic, A. Demessence, L. Cardenas, F. Maillard and A. Fateeva, *Chem. Commun.*, 2017, **53**, 6496–6499; (*c*) Z. H. Huang, N. H. Xie, M. Zhang and B. Q. Xu, *ChemSusChem*, 2019, **12**, 200–207; (*d*) H. X. Zhong, K. H. Ly, M. C. Wang, Y. Krupskaya, X. C. Han, J. C. Zhang, J. Zhang, V. Kataev, B. Bgchner, I. M. Weidinger, S. Kaskel, P. Liu, M. W. Chen, R. H. Dong and X. L. Feng, *Angew. Chem., Int. Ed.*, 2019, **58**, 10677–10682; (*e*) F. H. Sun and X. Chen, *Electrochem. Commun.*, 2017, **82**, 89–92; (*f*) Y. Zhou, Y. F. Xing, J. Wen, H. B. Ma, F. B. Wang and X. H. Xia, *Sci. Bull.*, 2019, **64**, 1158–1166; (*g*) N. Ramaswamy, U. Tylus, Q. Jia and S. Mukerjee, *J. Am. Chem. Soc.*, 2013, **135**, 15443–15449.

24 (*a*) H. Y. He, M. Wang, J. S. Zhao and Y. Zhang, *Chem. Eng. J.*, 2017, **316**, 680–691; (*b*) L. Gu, Y. Chu, H. M. Du, Y. Zhang, J. S. Zhao and Y. Xie, *Front. Chem.*, 2019, **7**, 622; (*c*) Y. Y. Zhao, Y. Chu, X. P. Ju, J. S. Zhao, L. Q. Kong and Y. Zhang, *Catalysts*, 2018, **8**, 53; (*d*) Y. Q. Lu, X. L. Wang, M. Wang, L. Q. Kong and J. S. Zhao, *Electrochim. Acta*, 2015, **180**, 86–95; (*e*) Y. Chu, L. Gu, H. H. Du, K. G. Qu, Y. Zhang, J. S. Zhao and Y. Xie, *Int. J. Hydrogen Energy*, 2018, **43**, 21810–21823.

25 (*a*) R. Bashyam and P. Zelenay, *Nature*, 2006, **443**, 63–66; (*b*) W. J. Jiang, L. Gu, L. Li, Y. Zhang, X. Zhang, L. J. Zhang, J. Q. Wang, J. S. Hu, Z. D. Wei and L. J. Wan, *J. Am. Chem. Soc.*, 2016, **138**, 3570–3578; (*c*) K. Iwase, T. Yoshioka, S. Nakanishi, K. Hashimoto and K. Kamiya, *Angew. Chem., Int. Ed.*, 2015, **54**, 11068–11072; (*d*) M. Kato, K. Kimijima, M. Shibata, H. Notsu, K. Ogino, K. Inokuma, N. Ohta, H. Uehara, Y. Uemura, N. Oyaizu, T. Ohba, S. Takakusagi, K. Asakura and I. Yagi, *Phys. Chem. Chem. Phys.*, 2015, **17**, 8638–8641; (*e*) Y. Y. Sun, L. Silvioli, N. R. Sahraie, W. Ju, J. K. Li, A. Zitolo, S. Li, A. Bagger, L. Arnarson, X. L. Wang, T. Moeller, D. Bernsmeier, J. Rossmeisl, F. Jaouen and P. Strasser, *J. Am. Chem. Soc.*, 2019, **141**, 12372–12381.

